

Deep Injective Prior for Inverse Scattering

AmirEhsan Khorashadizadeh¹, Sepehr Eskandari², Vahid Khorashadi-Zadeh³ and Ivan Dokmanić⁴

Abstract—In electromagnetic inverse scattering, we aim to reconstruct object permittivity from scattered waves. Deep learning is a promising alternative to traditional iterative solvers, but it has been used mostly in a supervised framework to regress the permittivity patterns from scattered fields or back-projections. While such methods are fast at test-time and achieve good results for specific data distributions, they are sensitive to the distribution drift of the scattered fields, common in practice. If the distribution of the scattered fields changes due to changes in frequency, the number of transmitters and receivers, or any other real-world factor, an end-to-end neural network must be re-trained or fine-tuned on a new dataset. In this paper, we propose a new data-driven framework for inverse scattering based on deep generative models. We model the target permittivities by a low-dimensional manifold which acts as a regularizer and learned from data. Unlike supervised methods which require both scattered fields and target signals, we only need the target permittivities for training; it can then be used with any experimental setup. We show that the proposed framework significantly outperforms the traditional iterative methods especially for strong scatterers while having comparable reconstruction quality to state-of-the-art deep learning methods like U-Net.

I. INTRODUCTION

ELECTROMAGNETIC inverse scattering is the problem of determining the electromagnetic properties of unknown objects from how they scatter incident fields. As it is non-destructive, it has a variety of applications in different areas, such as early detection of breast cancer [1], mineral prospecting [2], detecting defects and cracks inside objects [3], imaging through the wall [4] and remote sensing [5].

We consider the reconstruction of the finite number of parameters of the object from the scattered fields. While inverse scattering is well-posed and Lipschitz stable in theory, when full-aperture continuous measurements are available [6], it is

a severely ill-posed inverse problem for a finite number of measurements. This means that a small perturbation in the scattered fields may lead to a large error in the reconstructed permittivity pattern [7]. Moreover, the forward operator from the permittivity to the scattered fields is nonlinear, which further complicates the inversion. The nonlinearity is due to the multiple scattering; the problem becomes more nonlinear as the permittivity contrast increases [7]. All these together make the inverse scattering challenging, especially for strong scatterers (objects with large permittivity) and noisy measurements, which require an effective regularization to restrict the search space and enable accurate reconstruction.

A number of optimization-based methods are proposed to address nonlinearity and ill-posedness of the inverse scattering including Born iterative [8], distorted Born iterative method (DBIM) [9], contrast source inversion (CSI) [10], and subspace-based optimization (SOM) [11]. Although these methods have been shown to be effective for objects with small permittivity, they do not give an accurate reconstruction for large permittivity. All the above methods iteratively optimize a regularized objective, with a hand-crafted regularization term.

Recently, thanks to the significant increase in computing power and the availability of sufficient data, data-driven approaches to inverse scattering have started receiving attention. Most deep learning models for inverse scattering use a *supervised* learning approach, which takes the scattered fields or a simple back-projection as input and trains a deep neural network to produce the target permittivity pattern. The authors of [12]–[14] used scattered fields as input. While this approach provides good reconstructions even for objects with strong scatterers [14], it is sensitive to the experiment configuration such as the frequency or the number of incident waves and receivers; if the distribution of the scattered fields in test-time slightly changes, the quality of reconstructions remarkably degrades; the model requires new training data which is too costly. One strategy to tackle this issue is to use back-projections as input instead of the raw scattered fields, thus enabling the use of convolutional neural networks [15]–[17]. While this approach is shown to be effective for objects with small and moderate permittivity, the quality of the back-projections significantly drops in large permittivity (Figure 3), which leads to a drop in the reconstruction quality [14]. On the other hand, supervised learning methods are also potentially vulnerable to adversarial attacks [18], which is problematic in medical applications [19]. Moreover, incorporating the well-known physics of the scattering problem (forward operator), which can strikingly improve the accuracy of the reconstructions, is not easy in supervised learning models [20].

Manuscript received December 29, 2022.

AmirEhsan Khorashadizadeh and Ivan Dokmanić were supported by the European Research Council Starting Grant 852821–SWING.

AmirEhsan Khorashadizadeh is with the Department of Mathematics and Computer Science of the University of Basel, 4001 Basel, Switzerland (e-mail: amir.kh@unibas.ch).

Sepehr Eskandari is with Microwave Systems, Sensors, and Imaging Lab (MiXIL), University of Southern California, Los Angeles, CA 90089 USA (e-mail: sepehres@usc.edu).

Vahid Khorashadi-Zadeh is with School of Electric and Computer Engineering, University of Tehran, Tehran 14399-57131, Iran (e-mail: v.khorashadi@ut.ac.ir).

Ivan Dokmanić is with the Department of Mathematics and Computer Science of the University of Basel, 4001 Basel, Switzerland, and also with the Department of Electrical, Computer Engineering, the University of Illinois at Urbana-Champaign, Urbana, IL 61801 USA (e-mail: ivan.dokmanic@unibas.ch).

Our implementation is available at https://github.com/swing-research/scattering_injective_prior.

To tackle these issues, we propose a deep learning approach to inverse scattering using *injective* generative models. The proposed method benefits from an unsupervised learning framework—the training phase uses only the target permittivity patterns and the physics of scattering is fully incorporated into the solution. Deep generative models are a class of unsupervised learning methods that model the probability distribution of data by using deep neural networks. Latent-variable generative models such as generative adversarial networks (GAN) [21], [22], variational autoencoders [23], normalizing flows [24]–[26] and diffusion models [27] train a deep neural network to transform the samples of a simple (Gaussian) distribution to those of target data distribution. We expect a trained generator produce plausible samples similar to the training data when taking samples of a Gaussian distribution as input.

Bora et al. [28] used GANs to constrain the solution domain to the range of the trained generator for solving compressed sensing inverse problems. The strength of this idea is that it requires only the target signals for training and does not know anything about the inverse problem is going to be solved. As soon as the generator is trained, it can be used to solve any inverse problem with a known forward operator. This property makes the model robust to the distribution shift of the measurements and adversarial attack.

Several methods have tried to improve the quality of reconstructions; Kelkar et al. [29] used the popular style-GAN generator [30] while Hussein et al. [31] jointly optimize the generator weights with latent codes to further reduce the reconstructions error. However, GANs are known to be unstable in training, and the optimization process over latent space sticks in the local minimum which requires many restarts [28]. Recently, normalizing flows as a generator instead of GANs have been shown to have a stable optimization landscape [32], [33]. Nevertheless, normalizing flows have their own drawbacks; having a latent code with the same dimension as data space makes them too expensive in training and does not provide an appropriate constraint in the generator output, leading to poor reconstruction for ill-posed inverse problems. More recently, injective normalizing flows [34], [35] are proposed to alleviate these issues. Injective flows are a class of deep generative models that are well-suited for solving ill-posed inverse problems. These models unlike GANs give us access to the approximate likelihood of the generated samples, which provides a likelihood-based regularization. Moreover, injective flows unlike regular normalizing flows benefit from a low-dimensional latent space which provides an additional effective regularizer for ill-posed inverse problems. Injective flows have been shown in [35] to effectively solve linear inverse problems.

In this paper, we use injective flows as the generator to solve full-wave inverse scattering. we will show that the proposed method effectively solves inverse scattering even for objects with large permittivity for which traditional methods fail. Moreover, we use a data-driven initial guess for starting the iterative optimization, which significantly outperforms the simple back-projection initialization used in the traditional

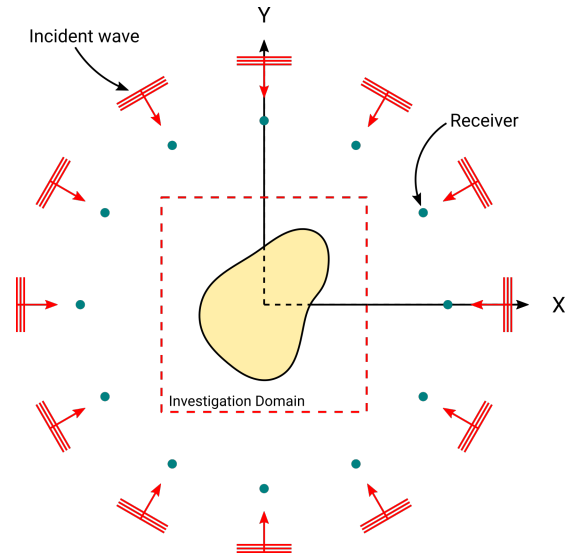


Fig. 1: The setup for the inverse scattering problem, red arrows show the incident plane waves; the green circles are the receivers.

methods. Finally, we show that the proposed framework yields reconstructions of comparable or better quality to highly successful supervised methods like the U-Net [36].

II. FORWARD AND INVERSE SCATTERING

We begin our discussion with equations governing the 2D forward and inverse scattering problem. We consider two-dimensional transverse magnetic scattering, where the longitudinal direction is along the z direction (TM_z). As shown in Figure 1, non-magnetic scatterers with permittivity ϵ_r in a vacuum background with permittivity ϵ_0 and permeability μ_0 are located in investigation domain \mathcal{D}_{inv} which is a $D \times D$ square, and are illuminated by N_i plane waves with equispaced directions. We have N_r receivers placed uniformly on a circle S with radius R which measure the scattered fields. The forward scattering problem can be derived from the time-harmonic form of Maxwell's equations and stated as [37],

$$\nabla \times (\nabla \times E^t(r)) - k_0^2 \epsilon_r(r) E^t(r) = i\omega \mu_0 J(r) \quad (1)$$

where E^t is the total electric field, $k_0 = \omega \sqrt{\mu_0 \epsilon_0}$ is the wavenumber of the homogeneous background and J is the contrast current density and can be calculated using equivalence theorem [38] as $J(r) = \chi(r) E^t(r)$ where $\chi(r) = \epsilon_r(r) - 1$ and is called the contrast. The time-dependence factor $\exp(i\omega t)$ with angular working frequency ω is assumed and will be suppressed throughout this paper. By using Dyadic Green's function [39], Equation (1) can be formalized by two coupled integral equations. The first one, called *Lippmann–Schwinger equation*, relates total electric fields E^t in an unknown domain to contrast current density J ,

$$E^t(r) = E^i(r) + k_0^2 \int_{\mathcal{D}_{inv}} g(r, r') J(r') dr', \quad (2)$$

where $r \in \mathcal{D}_{inv}$, and

$$g(r, r') = \frac{1}{4i} H_0^{(2)}(k_0 |r - r'|),$$

and $H_0^{(2)}$ is the Hankel function of the second kind, denotes 2D free space Green's function. The second equation, referred to as the *data equation*, maps the contrast current density J to the scattered electric fields E^s at the receivers locations,

$$E^s(r) = k_0^2 \int_{\mathcal{D}_{inv}} g(r, r') J(r') dr', \quad r \in S. \quad (3)$$

We discretize the investigation domain \mathcal{D}_{inv} with $N \times N$ units and rewrite Equations (2) and (3) as

$$\begin{aligned} E^t &= E^i + G_d \chi E^t \\ E^s &= G_s \chi E^t + \delta \end{aligned} \quad (4)$$

where $G_d \in \mathbb{R}^{N^2 \times N^2}$ and $G_s \in \mathbb{R}^{N_r \times N^2}$ have analytical closed form [7]. Moreover, E^t , E^i and E^s respectively correspond to total, incident and scattered electric fields and χ is a diagonal matrix with the diagonal elements $\chi(n, n) = \epsilon_r(r_n) - 1$. We also consider additive noise δ to the measurements.

We merge Equations (4) and (5) to make a single expression for the forward equation [7],

$$E^s = G_s \chi (I - G_d \chi)^{-1} E^i + \delta, \quad (6)$$

which is a nonlinear mapping $\chi \mapsto E^s$. It is convenient to define a forward operator A mapping χ to E^s ,

$$y = A(x) + \delta, \quad (7)$$

where $A(\cdot)$ is the nonlinear forward scattering operator

$$A(\chi) = G_s \chi (I - G_d \chi)^{-1} E^i, \quad (8)$$

$y = E^s$ and $x = \chi$. The task of inverse scattering is to reconstruct the contrast signal χ from the scattered fields E^s where we assume G_d , G_s , incident electric waves E^i and consequently the forward operator $A(\cdot)$ are known. In the next section, we briefly review deep generative models as the prior model for inverse problems.

III. DEEP GENERATIVE MODELS

One major division in machine learning is generative and discriminative models. In discriminative models, one aims to learn a direct mapping from the measurements to the target signals. Discriminative approaches have been extensively used in solving inverse problems, specifically U-Net [36] has shown great success in many applications such as computed tomography (CT) [40], magnetic resonance imaging (MRI) [41], optoacoustic tomography [42] and electromagnetic inverse scattering [16]. The key idea of this success might be ascribed to having a multiscale architecture [43]. Recently, the variational version of U-Net has shown excellent performance for posterior sampling and uncertainty quantification of inverse scattering problem [44].

On the other hand, the task of generative models is to learn the probability distribution of data. Latent-variable generative models including generative adversarial networks (GANs) [21], [22], variational autoencoders [23] and normalizing flows [24]–[26] are a subcategory of deep generative models (DGMs) which train a deep neural network, called the generator, to transform the samples of a simple and known distribution (often Gaussian) to data distribution samples. DGMs have many applications such as image generation [22], image-to-image translation [45], density estimation [46] and variational inference [47], [48]. Recently, DGMs have been used as a prior for solving inverse problems [28], [35], [49]–[52]; consider a DGM trained on a training set of target signals (the solutions of a given inverse problem), one can search in the latent space of the trained generator for the latent code yielding a solution aligns with the given measurements. The pre-trained generator plays the role of an effective regularizer for generating plausible target signals. As discussed earlier, the key advantage of this approach is that the measurements are not used in the training phase. As a result, once the DGM is trained, it can be used for solving any inverse problems.

However, the choice of DGM is of paramount importance to provide stable training, high-quality sample generation, and an effective regularizer for solving *ill-posed* inverse problems. While modern GANs with the various innovations in architectures and training protocols exhibit high-quality samples, they suffer from training instability [53], [54] and have shown poor reconstructions when used as a prior for solving ill-posed inverse problems [35], [55]. Normalizing flows alleviates many drawbacks of GAN; they are stable in training and can produce high-quality samples. Normalizing flows comprise a set of bijective transformations which have tractable inverse and log det Jacobian computations. They give access to the likelihood of the generated samples and can be trained based on maximum likelihood. Normalizing flows as a prior were shown to be more effective than GANs for solving inverse problems [32], [33]. However unlike GANs, normalizing flows are bijective mappings, having the same dimension in the latent space and data space, consequently, the network output is not constraint and leading to poor regularization for solving ill-posed inverse problems [14].

More recently, the authors of [35] showed that injective normalizing flows are so effective for solving ill-posed inverse problems. Injective normalizing flows are an extension of normalizing flows which have a low-dimensional latent space. Injective flows provide a low-dimensional representation of the data (like GANs) which perform as a strong regularization for solving inverse problems while giving access to the likelihood of the generated samples (like normalizing flows) which can be seen as the second regularization. In the next section, we briefly review injective flows called Trumpets.

IV. INJECTIVE NORMALIZING FLOWS

Injective normalizing flows [35] map a low-dimensional latent space to the high-dimensional data space using a set of

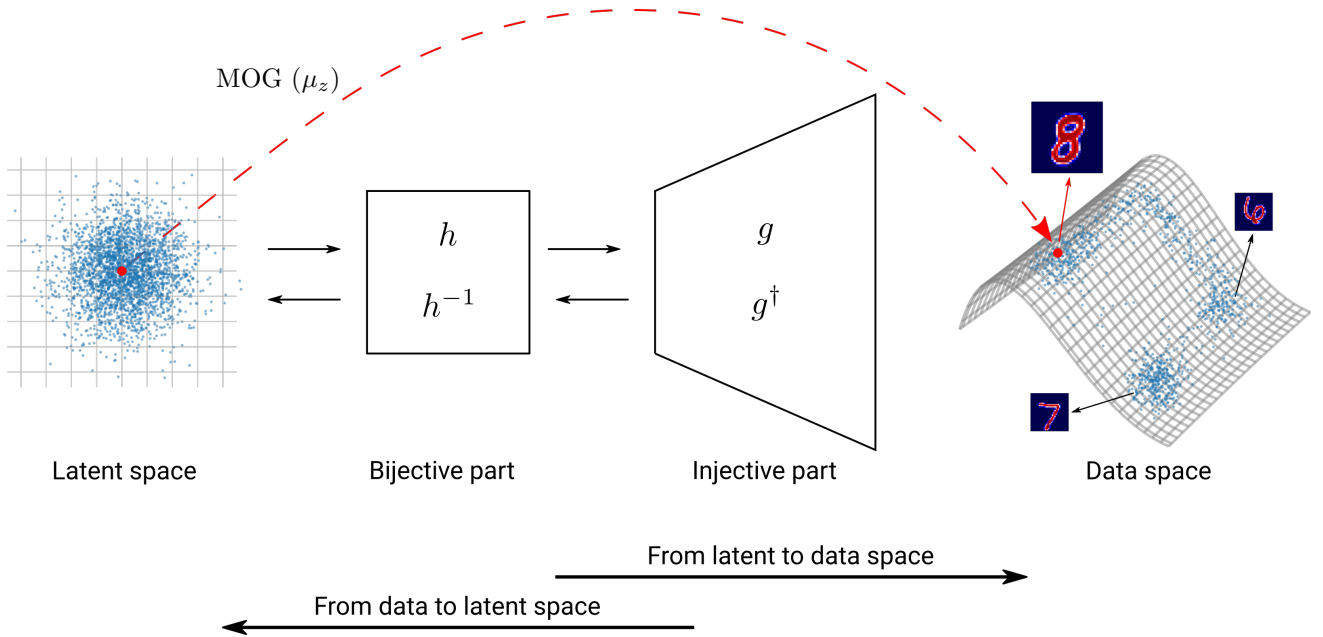


Fig. 2: Injective normalizing flows [35] comprise two submodules, a low-dimensional bijective flow h_η and an injective network with expansive layers g_γ . The MOG initialization is the mean of the Gaussian in the latent space $z_{init} = \mu_z$ (red circle).

invertible neural networks. Injective normalizing flows have a fast inverse on the range and give access to the likelihood of the generated samples. As shown in Figure 2, $f_\theta(z) = g_\gamma(h_\eta(z))$ with weights $\theta = (\gamma, \eta)$ comprises two subnetworks: an injective part (with expansive layers) g_γ that maps a low-dimensional space \mathbb{R}^d to high-dimensional data space \mathbb{R}^D where $d \ll D$, and a bijective mapping h_η that keeps the dimension in low dimensional space \mathbb{R}^d . The training of the injective normalizing flows consists of two phases, at first, the range of the injective generator must be adjusted to lie on the training data by optimizing over the weights of the injective subnetwork g_γ , when we ensure the training data are close to the range of the generator, in the second phase the likelihood of the pre-image of the training data should be maximized over the weights of the bijective subnetwork h_η . Further details are explained in [35]. When the network is trained, we can generate random samples similar to the training data

$$x_{\text{gen}} = f(z_{\text{gen}}) \quad (9)$$

where $z_{\text{gen}} \sim \mathcal{N}(\mu_z, \sigma_z^2 I)$. Further information about the universality of density and manifold approximation of injective normalizing flows are studied in [56].

Due to having a low-dimensional latent space, injective flows provide a low-dimensional manifold in the high-dimensional data space. When they are trained, the manifold would contain plausible samples which can be used as an effective regularizer for solving ill-posed inverse problems. The injective part provides a projection operator $g_\gamma(g_\gamma^\dagger(x))$ which maps the data samples x to the intermediate space by $z' = g_\gamma^\dagger(x)$ and projects them back to the data space by $g_\gamma(z')$. The authors of [35] used the projection operator to project a sample on the manifold to suppress the noise and artifacts, as the learned manifold contains high-quality samples. In the

next section, we will present our method of solving inverse scattering problems using injective normalizing flows.

V. INJECTIVE FLOWS FOR INVERSE SCATTERING

Inverse scattering is a severely ill-posed inverse problem, which means a small perturbation in the scattered fields leads to an exponentially large error in the contrast [7]. This makes the inversion unstable even for a small amount of noise. As discussed in section II, inverse scattering is a nonlinear inverse problem whose nonlinearity heavily relies on the maximum contrast value. For objects with large contrasts, the problem becomes highly nonlinear, which makes the inversion extremely difficult. In such a scenario, the significance of having a strong regularizer to restrict the search domain is crucially important.

We consider the contrast signal $\chi = x \in \mathcal{X}$ and the scattered fields $E^s = y \in \mathcal{Y}$, described by forward operator (7), as random vectors. While our framework admits other distributions beyond Gaussian for the additive noise δ in (7), in this paper we assume that δ is a random vector with Gaussian distribution $\delta \sim \mathcal{N}(0, \sigma^2 I)$ yielding

$$Y|X \sim \mathcal{N}(A(X), \sigma^2 I). \quad (10)$$

One effective approach for solving ill-posed inverse problems is computing MAP estimate, where we look for the solution x that has the highest posterior likelihood for a given measurement y ,

$$x_{\text{MAP}} = \arg \max_x \log(p_{X|Y}(x|y)), \quad (11)$$

where $p_{X|Y}(x|y)$ is the posterior distribution for the given measurement y . Using Bayes theorem yields,

$$\begin{aligned} x_{\text{MAP}} &= \arg \min_x -\log(p_{X|Y}(x|y)) \\ &= \arg \min_x -\log\left(\frac{p_{Y|X}(y|x)p_X(x)}{p_Y(y)}\right) \\ &= \arg \min_x -\log(p_{Y|X}(y|x)) - \log(p_X(x)). \end{aligned} \quad (12)$$

The first term can be obtained from (10),

$$x_{\text{MAP}} = \arg \min_x \frac{1}{2} \|y - A(x)\|_2^2 - \lambda \log(p_X(x)), \quad (13)$$

where the first term is the data-consistency loss while $\log(p_X(x))$ is the prior distribution of the contrast and plays the role of the regularization. We also have λ which is a hyperparameter to adjust the amount of regularization term (although it comes from the noise standard deviation which we assume is unknown). In principle, the prior distribution $p_X(x)$ is not available and must be estimated. For example, traditionally $p_X(x)$ is approximated with a Gaussian distribution with zero mean leading to the Tikhonov regularization. However, a Gaussian distribution is often too far from the true prior distribution and leads to poor reconstructions.

In this paper, we study a new regularization family for inverse scattering based on deep generative models. We consider a training set of contrast signals $\{x^{(i)}\}_{i=1}^N$ is available, and we train a deep generative model $x = f(z)$ to produce high-quality contrast samples. we expect the trained generator f to produce high-quality contrast samples when it takes random samples from the Gaussian distribution in the latent space $z \in \mathcal{Z}$. As discussed in section III, this property of deep generative models makes them an effective regularizer for solving inverse problems [28].

We use injective normalizing flows as the generator of the contrast signal since they are well-suited for solving ill-posed inverse problems [35]. We perform an optimization in the latent space to find the latent code that aligns with scattered fields y ,

$$z_{\text{MAP}} = \arg \max_z \frac{1}{2} \|y - A(f(z))\|_2^2 + \lambda \log(p_X(f(z))), \quad (14)$$

Where an approximation to p_X is also provided by the injective flows and acts as the second regularizer. The reconstructed contrast signal can be obtained as $x_{\text{MAP}} = f(z_{\text{MAP}})$. We call this method latent space optimization (LSO). It is worth mentioning that (14) has been previously proposed by [32], [33] for solving compressed sensing inverse problems using regular normalizing flows.

Unlike the supervised learning methods for inverse scattering [13], [15]–[17] which use a paired training set of contrast and scattered fields $\{(x^{(i)}, y^{(i)})\}_{i=1}^N$, our framework benefits from an unsupervised learning paradigm where scattered fields are not used in the training of injective flows. This means, if the distribution of the scattered fields changes (due to the change in experimental configuration), the generative network is not required to be retrained unlike the supervised methods; as soon as the injective generator is trained over the contrast signals, we can optimize (14) for each new scattered fields to reconstruct

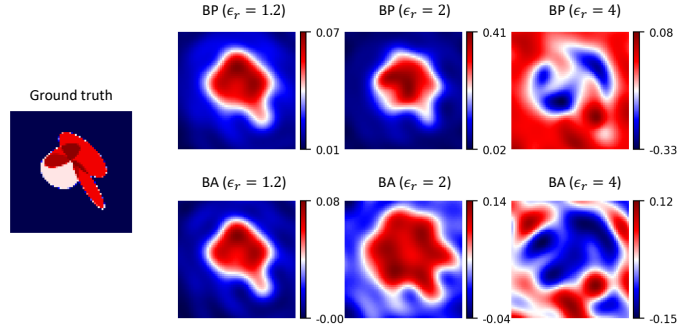


Fig. 3: Performance analysis of back-propagation (BP) and Born approximation (BA) methods for different ϵ_r ; while BA and BP reconstructions are visually meaningful for small ϵ_r , their performance sharply drop for objects with large ϵ_r .

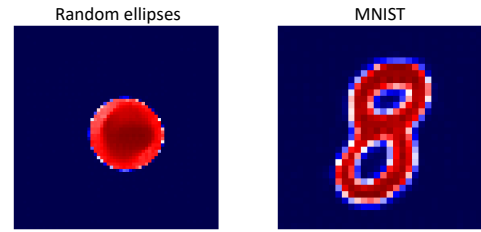


Fig. 4: Illustration of the MOG initializer in the data space $f(\mu_z)$ for random ellipses and MNIST datasets

the corresponding contrast. Apart from the advantages of an unsupervised learning paradigm, the proposed method fully exploits the underlying physics of the scattering problem by optimizing over the complex-valued scattered fields in (14). Kothari et al. [57] have shown incorporating wave physics in the neural network architecture can significantly improve the quality of reconstructions, especially for out-of-distribution data.

We solve the optimization problem (14) by Adam optimizer [58] and compute the gradients with respect to z by automatic differentiation provided by TensorFlow [59] in Python. We also use an alternative method for Equation (14) proposed by [35] which performs the optimization in the data space,

$$x_{\text{MAP}} = \arg \min_x \frac{1}{2} \|y - A(g^\dagger(x))\|_2^2 - \lambda \log(p_X(x)) \quad (15)$$

where $g^\dagger(x)$ is the projection operator explained in section IV. We call this method data space optimization (DSO). This method is shown in [35] to be effective for solving linear inverse problems. While in each of the LSO iterations the reconstructed point $x = f(z)$ is always on the learned manifold, this is not the case for the DSO method, where the reconstructed image might be off the manifold. Moreover, the DSO method requires more computations than LSO as we need to take derivatives over the reverse direction of the injective subnetwork $g^\dagger(x)$.

The choice of initial guess is crucially important in inverse

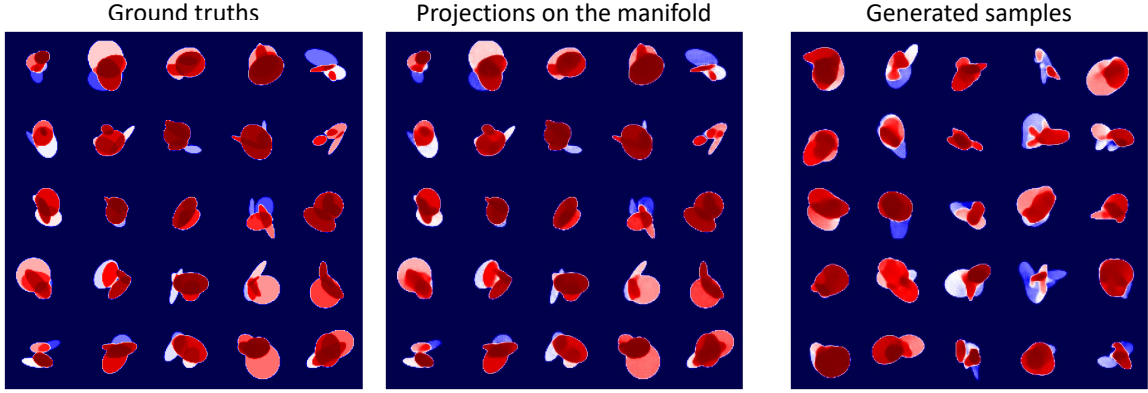


Fig. 5: Performance evaluation of the trained injective normalizing flows for random ellipses dataset; ground truth contrasts, their projections on the learned manifold and some randomly generated samples.

scattering solvers. While a poor initialization misleads the optimization process, a good initial step helps the algorithm to converge more accurately and faster. The authors of [9] used Born approximation as the initialization for the distorted Born iterative method (DBIM). A back-propagation (BP) solution was also used in [10], [60] as an initial guess of the contrast source inversion (CSI) method. Figure 3 shows the ground truth, back-propagation (BP) and Born approximations (BA) for an object with different maximum ϵ_r values. While BP and BA can present fuzzy reconstructions for objects with small permittivity, their performance sharply drops for large ϵ_r (especially numerically) which makes them a poor initialization for strong scatterers.

In order to circumvent this issue, we use a data-driven initialization suggested in [32]; mean of the Gaussian distribution (MOG) in the latent space as shown in Figure 2. The MOG initializer $z_{\text{init}} = \mu_z$ provides a fixed initialization with respect to the measurements (scattered fields); thereby being independent of the maximum contrast value and the problem configuration. This property helps (14) and (15) to converge better even for a large ϵ_r . In section VI, we will show that MOG initialization significantly improves the quality of the reconstructions compared to BP. To our best knowledge, this is the first time that we propose a data-driven initializer for inverse scattering.

VI. COMPUTATIONAL EXPERIMENTS

In the following, we will evaluate the performance of DSO and LSO for inverse scattering. We consider the MOG and BP initializations for DSO while using just MOG initialization for LSO. We compare the performance of our proposed methods with a traditional iterative method DBIM [9]. While our method is based on an unsupervised-learning paradigm; scattered fields are not used during training, we also compare its performance with a successful supervised learning method, U-Net [36] which has shown great success for inverse scattering [16], to show the effectivity of our method. U-Net takes the back-propagation

(BP) as input and returns the permittivity pattern of the object in the output.

We use MNIST [61] with 60000 training samples in the resolution $N = 32$. We also use a custom dataset of 60000 training samples with resolution $N = 64$ of overlapping ellipses used in [14] to have a more challenging task for accurate reconstructions.

We use $N_i = 12$ incident plane waves and $N_r = 12$ receivers, uniformly distributed on a circle with radius $R = 20$ cm around the object with maximum permittivity ϵ_r and dimension $D = 20$ cm. The working frequency is 3 GHz and we added 30 dB noise to the scattered fields.

We used the injective normalizing flows with the same architecture described in [35]. We trained the injective subnetwork g_γ for 150 epochs to ensure the training samples (contrast signals) are close to the range of the generator. Figure 5 shows some test samples and their projections on the learned manifold. Then we trained the bijective subnetwork h_η for 150 epochs to maximize the likelihood of the pre-image of the training samples in the intermediate space. Figure 5 illustrates some randomly generated samples which confirms that the model can produce plausible samples to be used as an effective prior for solving inverse scattering.

We optimize (14) and (15) by using Adam optimizer with a learning rate of 0.05 for 300 iterations. We use $\lambda = 0.01$ for BP and $\lambda = 0$ for MOG initialization. It is worth mentioning that when we use MOG initializer, we start from high-likelihood regions (mean of the Gaussian) which can be viewed as a hidden regularizer, we thus use $\lambda = 0$ in this case. Figure 4 shows the MOG initialization for MNIST and random ellipses datasets.

Figures 6 and 7 show the performance of different methods for inverse scattering for $\epsilon_r = 4$ over five test samples from random ellipses and MNIST datasets. While the traditional iterative method (DBIM) meets with complete failure in this challenging task ($\epsilon_r = 4$ and 30 dB noise), DSO and LSO have strikingly more accurate reconstructions, which clearly

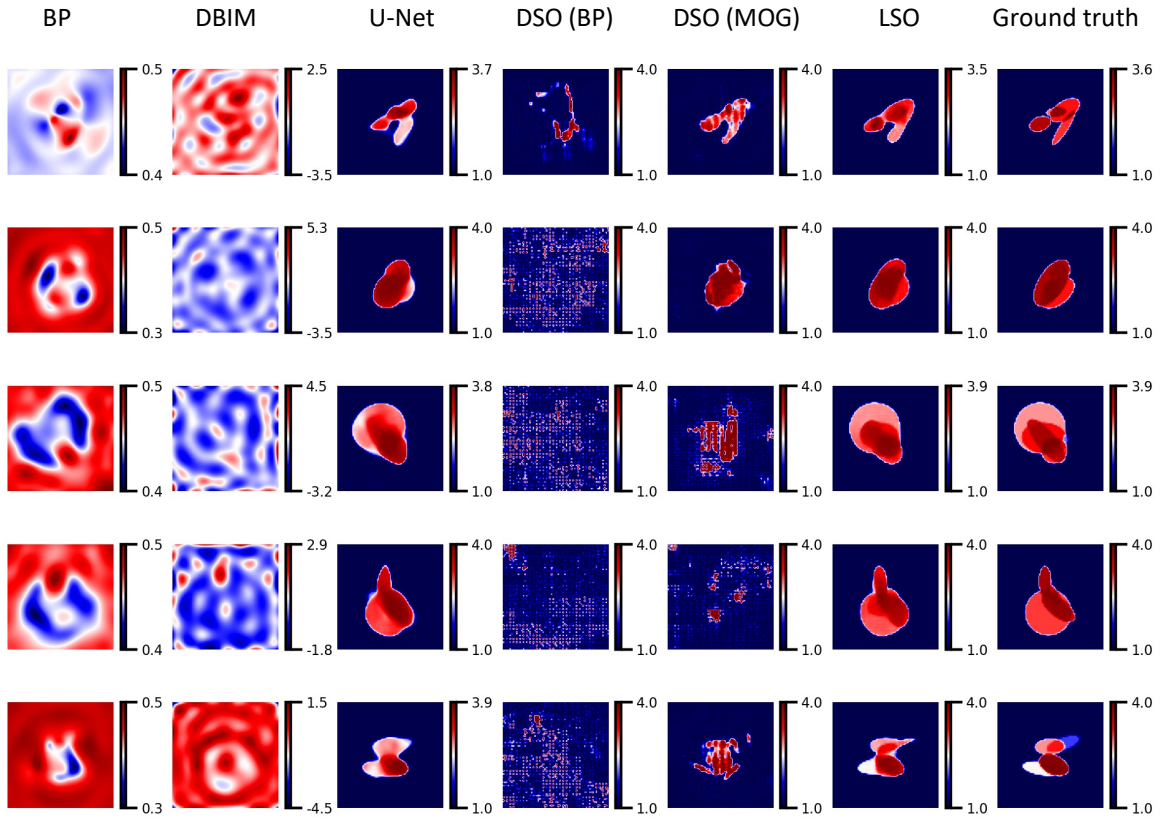


Fig. 6: Performance comparison of different methods over random ellipses dataset in resolution 64×64

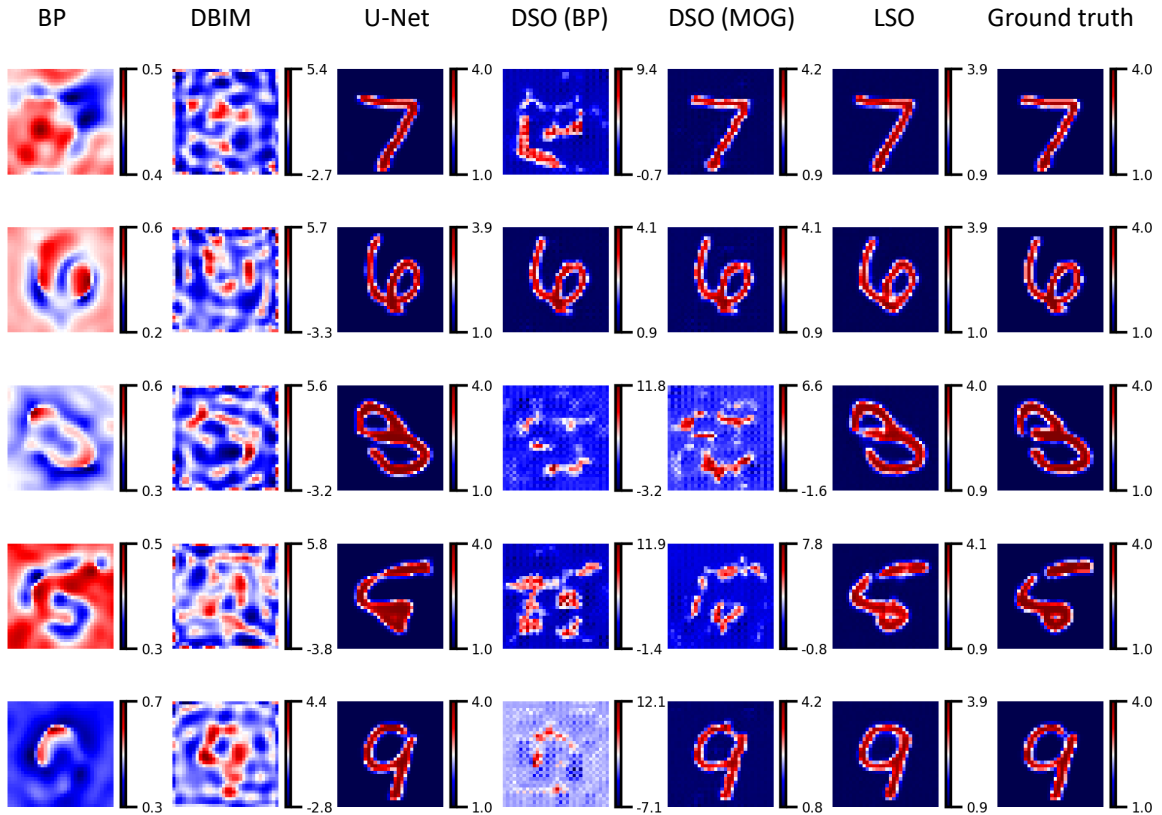


Fig. 7: Performance comparison of different methods over MNIST dataset in resolution 32×32

TABLE I: Performance of different methods for solving inverse scattering ($\epsilon_r = 4$) averaged over 25 test samples

	PSNR		SSIM	
	MNIST	Ellipses	MNIST	Ellipses
BP	7.75	7.00	0.01	0.01
DBIM [9]	5.77	4.67	0.01	0.01
U-Net [36]	24.26	21.94	0.90	0.82
DSO (BP)	8.73	7.89	0.16	0.16
DSO (MOG)	21.50	14.56	0.56	0.44
LSO (MOG)	25.22	20.50	0.89	0.85

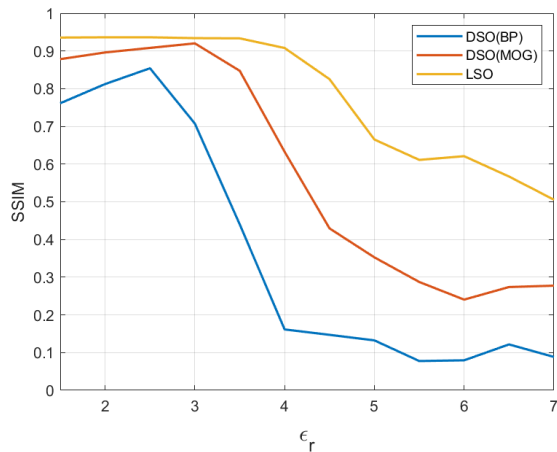


Fig. 8: The performance of different methods for different ϵ_r over MNIST dataset; SSIM is computed over the normalized signals between -1 and 1 .

shows the significance of a data-driven regularization. Moreover, the MOG initialization, as we expected, exhibits remarkably better reconstructions compared to BP for this high permittivity ($\epsilon_r = 4$). Furthermore, both figures show that LSO outperforms DSO; running optimization in the latent space results in better reconstructions as discussed in section V. Finally, while LSO does not use scattered fields in the training phase, it could present the reconstructions with comparable quality (or even better) to the highly successful supervised method U-Net. Table I shows the numerical results in PSNR and SSIM averaged over 25 test samples.

As discussed in section V, the maximum ϵ_r of the object plays a significant role in the performance of inverse scattering solvers; objects with large ϵ_r are more difficult to be reconstructed. Figure 8 demonstrates the performance of different methods per ϵ_r over the MNIST dataset. This figure discovers that LSO with MOG initialization is effective even for objects with large, ϵ_r which clearly signifies the power of a data-driven initialization and performing the optimization in the latent space.

VII. LIMITATIONS AND CONCLUSIONS

We proposed a learning-based framework for inverse scattering using an injective prior. The proposed method fully exploits the physical domain of the scattering problem while

benefiting from a data-driven initialization which makes a powerful solver even for objects with a large contrast. The invertible generator admits performing optimization in both latent and data space and uses a data-driven or back-projection as the initializer. We showed that performing optimization in the latent space and using the mean of the Gaussian as the initial guess significantly outperforms the traditional iterative methods and even gives reconstructions comparable to the successful supervised learning method, U-Net.

Limitations: The proposed framework has several limitations and entails discussion. It requires running an iterative method in test-time, which is slow and cannot be used for real-time applications. To speed up the convergence, one may consider a more accurate initial guess by exploiting the physical domain in the data-driven initializer; a combination of traditional back-projection (like BP) and the data-driven initializers (like MOG). Recently, Hussein et al. [31] optimized the generator weights with a small rate after finding the optimal latent code in Equation (14) to further improve the reconstructions. This idea might be taken in our framework to go beyond the quality of the generator, but we leave it for future works.

REFERENCES

- [1] N. K. Nikolova, "Microwave imaging for breast cancer," *IEEE microwave magazine*, vol. 12, no. 7, pp. 78–94, 2011. 1
- [2] A. Friedman, "Application of inverse scattering to oil field evaluation problems;" in *Mathematics in Industrial Problems*. Springer, 1998, pp. 169–178. 1
- [3] R. Zoughi, *Microwave non-destructive testing and evaluation principles*. Springer Science & Business Media, 2000, vol. 4. 1
- [4] V. Khorashadi-Zadeh and M. Dehmollaian, "Through a cinder block wall refocusing using sar back projection method," *IEEE Transactions on Antennas and Propagation*, vol. 67, no. 2, pp. 1212–1222, 2018. 1
- [5] Y.-Q. Jin, *Electromagnetic scattering modelling for quantitative remote sensing*. World Scientific, 1993. 1
- [6] A. I. Nachman, "Global uniqueness for a two-dimensional inverse boundary value problem," *Annals of Mathematics*, pp. 71–96, 1996. 1
- [7] X. Chen, *Computational methods for electromagnetic inverse scattering*. John Wiley & Sons, 2018. 1, 3, 4
- [8] Y. Wang and W. C. Chew, "An iterative solution of the two-dimensional electromagnetic inverse scattering problem," *International Journal of Imaging Systems and Technology*, vol. 1, no. 1, pp. 100–108, 1989. 1
- [9] W. C. Chew and Y.-M. Wang, "Reconstruction of two-dimensional permittivity distribution using the distorted born iterative method," *IEEE transactions on medical imaging*, vol. 9, no. 2, pp. 218–225, 1990. 1, 6, 8
- [10] P. M. Van Den Berg and R. E. Kleinman, "A contrast source inversion method," *Inverse problems*, vol. 13, no. 6, p. 1607, 1997. 1, 6
- [11] X. Chen, "Subspace-based optimization method for solving inverse-scattering problems," *IEEE Transactions on Geoscience and Remote Sensing*, vol. 48, no. 1, pp. 42–49, 2009. 1
- [12] Y. Khoo and L. Ying, "Switchnet: a neural network model for forward and inverse scattering problems," *SIAM Journal on Scientific Computing*, vol. 41, no. 5, pp. A3182–A3201, 2019. 1
- [13] P. Ran, Y. Qin, and D. Lesselier, "Electromagnetic imaging of a dielectric micro-structure via convolutional neural networks," in *2019 27th European Signal Processing Conference (EUSIPCO)*. IEEE, 2019, pp. 1–5. 1, 5
- [14] A. Khorashadizadeh, K. Kothari, L. Salsi, A. A. Harandi, M. de Hoop, and I. Dokmanić, "Conditional Injective Flows for Bayesian Imaging," *arXiv preprint arXiv:2204.07664*, 2022. 1, 3, 6
- [15] L. Li, L. G. Wang, F. L. Teixeira, C. Liu, A. Nehorai, and T. J. Cui, "DeepNIS: Deep neural network for nonlinear electromagnetic inverse scattering," *IEEE Transactions on Antennas and Propagation*, vol. 67, no. 3, pp. 1819–1825, 2018. 1, 5

- [16] Z. Wei and X. Chen, "Deep-learning schemes for full-wave nonlinear inverse scattering problems," *IEEE Transactions on Geoscience and Remote Sensing*, vol. 57, no. 4, pp. 1849–1860, 2018. **1, 3, 5, 6**
- [17] J. E. Fajardo, J. Galván, F. Vericat, C. M. Carlevaro, and R. M. Irastorza, "Phaseless microwave imaging of dielectric cylinders: An artificial neural networks-based approach," *arXiv preprint arXiv:1908.10424*, 2019. **1, 5**
- [18] A. Madry, A. Makelov, L. Schmidt, D. Tsipras, and A. Vladu, "Towards deep learning models resistant to adversarial attacks," *arXiv preprint arXiv:1706.06083*, 2017. **1**
- [19] V. Antun, F. Renna, C. Poon, B. Adcock, and A. C. Hansen, "On instabilities of deep learning in image reconstruction and the potential costs of AI," *Proceedings of the National Academy of Sciences*, vol. 117, no. 48, pp. 30088–30095, 2020. **1**
- [20] X. Chen, Z. Wei, M. Li, and P. Rocca, "A review of deep learning approaches for inverse scattering problems (invited review)," *Progress In Electromagnetics Research*, vol. 167, pp. 67–81, 2020. **1**
- [21] I. Goodfellow, J. Pouget-Abadie, M. Mirza, B. Xu, D. Warde-Farley, S. Ozair, A. Courville, and Y. Bengio, "Generative adversarial nets," *Advances in neural information processing systems*, vol. 27, 2014. **2, 3**
- [22] A. Radford, L. Metz, and S. Chintala, "Unsupervised representation learning with deep convolutional generative adversarial networks," *arXiv preprint arXiv:1511.06434*, 2015. **2, 3**
- [23] D. P. Kingma and M. Welling, "Auto-encoding variational Bayes," *arXiv preprint arXiv:1312.6114*, 2013. **2, 3**
- [24] L. Dinh, D. Krueger, and Y. Bengio, "Nice: Non-linear independent components estimation," *arXiv preprint arXiv:1410.8516*, 2014. **2, 3**
- [25] L. Dinh, J. Sohl-Dickstein, and S. Bengio, "Density estimation using real nvp," *arXiv preprint arXiv:1605.08803*, 2016. **2, 3**
- [26] D. P. Kingma and P. Dhariwal, "Glow: Generative flow with invertible 1×1 convolutions," *Advances in neural information processing systems*, vol. 31, 2018. **2, 3**
- [27] J. Ho, A. Jain, and P. Abbeel, "Denosing diffusion probabilistic models," *Advances in Neural Information Processing Systems*, vol. 33, pp. 6840–6851, 2020. **2**
- [28] A. Bora, A. Jalal, E. Price, and A. G. Dimakis, "Compressed sensing using generative models," in *International Conference on Machine Learning*. PMLR, 2017, pp. 537–546. **2, 3, 5**
- [29] V. A. Kelkar and M. Anastasio, "Prior image-constrained reconstruction using style-based generative models," in *International Conference on Machine Learning*. PMLR, 2021, pp. 5367–5377. **2**
- [30] T. Karras, S. Laine, and T. Aila, "A style-based generator architecture for generative adversarial networks," in *Proceedings of the IEEE/CVF conference on computer vision and pattern recognition*, 2019, pp. 4401–4410. **2**
- [31] S. A. Hussein, T. Tirer, and R. Giryas, "Image-adaptive gan based reconstruction," in *Proceedings of the AAAI Conference on Artificial Intelligence*, vol. 34, no. 04, 2020, pp. 3121–3129. **2, 8**
- [32] M. Asim, M. Daniels, O. Leong, A. Ahmed, and P. Hand, "Invertible generative models for inverse problems: mitigating representation error and dataset bias," in *International Conference on Machine Learning*. PMLR, 2020, pp. 399–409. **2, 3, 5, 6**
- [33] J. Whang, Q. Lei, and A. Dimakis, "Compressed sensing with invertible generative models and dependent noise," in *NeurIPS 2020 Workshop on Deep Learning and Inverse Problems*, 2020. **2, 3, 5**
- [34] J. Brehmer and K. Cranmer, "Flows for simultaneous manifold learning and density estimation," *Advances in Neural Information Processing Systems*, vol. 33, pp. 442–453, 2020. **2**
- [35] K. Kothari, A. Khorashadizadeh, M. de Hoop, and I. Dokmanić, "Trumpets: Injective flows for inference and inverse problems," in *Uncertainty in Artificial Intelligence*. PMLR, 2021, pp. 1269–1278. **2, 3, 4, 5, 6**
- [36] O. Ronneberger, P. Fischer, and T. Brox, "U-net: Convolutional networks for biomedical image segmentation," in *International Conference on Medical image computing and computer-assisted intervention*. Springer, 2015, pp. 234–241. **2, 3, 6, 8**
- [37] P. Y. Chen, D. J. Bergman, and Y. Sivan, "Spectral decomposition of the lippmann-schwinger equation applied to cylinders," *arXiv preprint arXiv:1705.01747*, 2017. **2**
- [38] S. R. Rengarajan and Y. Rahmat-Samii, "The field equivalence principle: Illustration of the establishment of the non-intuitive null fields," *IEEE Antennas and Propagation Magazine*, vol. 42, no. 4, pp. 122–128, 2000. **2**
- [39] H. Levine and J. Schwinger, "On the theory of electromagnetic wave diffraction by an aperture in an infinite plane conducting screen," *Communications on Pure and Applied Mathematics*, vol. 3, no. 4, pp. 355–391, 1950. **2**
- [40] K. H. Jin, M. T. McCann, E. Froustey, and M. Unser, "Deep convolutional neural network for inverse problems in imaging," *IEEE Transactions on Image Processing*, vol. 26, no. 9, pp. 4509–4522, 2017. **3**
- [41] C. M. Hyun, H. P. Kim, S. M. Lee, S. Lee, and J. K. Seo, "Deep learning for undersampled mri reconstruction," *Physics in Medicine & Biology*, vol. 63, no. 13, p. 135007, 2018. **3**
- [42] N. Davoudi, X. L. Deán-Ben, and D. Razansky, "Deep learning optoacoustic tomography with sparse data," *Nature Machine Intelligence*, vol. 1, no. 10, pp. 453–460, 2019. **3**
- [43] T. Liu, A. Chaman, D. Belius, and I. Dokmanic, "Learning multiscale convolutional dictionaries for image reconstruction," *IEEE Transactions on Computational Imaging*, 2022. **3**
- [44] A. Khorashadizadeh, A. Aghababaei, T. Vlašić, H. Nguyen, and I. Dokmanić, "Deep variational inverse scattering," *arXiv preprint arXiv:2212.04309*, 2022. **3**
- [45] J.-Y. Zhu, T. Park, P. Isola, and A. A. Efros, "Unpaired image-to-image translation using cycle-consistent adversarial networks," in *Proceedings of the IEEE international conference on computer vision*, 2017, pp. 2223–2232. **3**
- [46] Q. Liu, J. Xu, R. Jiang, and W. H. Wong, "Density estimation using deep generative neural networks," *Proceedings of the National Academy of Sciences*, vol. 118, no. 15, 2021. **3**
- [47] D. Rezende and S. Mohamed, "Variational inference with normalizing flows," in *International conference on machine learning*. PMLR, 2015, pp. 1530–1538. **3**
- [48] G. Papamakarios, E. Nalisnick, D. J. Rezende, S. Mohamed, and B. Lakshminarayanan, "Normalizing flows for probabilistic modeling and inference," *Journal of Machine Learning Research*, vol. 22, no. 57, pp. 1–64, 2021. **3**
- [49] G. Ongie, A. Jalal, C. A. Metzler, R. G. Baraniuk, A. G. Dimakis, and R. Willett, "Deep learning techniques for inverse problems in imaging," *IEEE Journal on Selected Areas in Information Theory*, vol. 1, no. 1, pp. 39–56, 2020. **3**
- [50] B. Kawar, M. Elad, S. Ermon, and J. Song, "Denosing diffusion restoration models," *arXiv preprint arXiv:2201.11793*, 2022. **3**
- [51] T. Vlašić, H. Nguyen, A. Khorashadizadeh, and I. Dokmanić, "Implicit neural representation for mesh-free inverse obstacle scattering," *arXiv preprint arXiv:2206.02027*, 2022. **3**
- [52] A. Khorashadizadeh, A. Chaman, V. Debarnot, and I. Dokmanić, "Funknn: Neural interpolation for functional generation," *arXiv preprint arXiv:2212.14042*, 2022. **3**
- [53] H. Thanh-Tung and T. Tran, "Catastrophic forgetting and mode collapse in gans," in *2020 International Joint Conference on Neural Networks (IJCNN)*. IEEE, 2020, pp. 1–10. **3**
- [54] M. Arjovsky and L. Bottou, "Towards principled methods for training generative adversarial networks," *arXiv preprint arXiv:1701.04862*, 2017. **3**
- [55] J. Whang, Q. Lei, and A. Dimakis, "Solving inverse problems with a flow-based noise model," in *International Conference on Machine Learning*. PMLR, 2021, pp. 11146–11157. **3**
- [56] M. Puthawala, M. Lassas, I. Dokmanić, and M. de Hoop, "Universal joint approximation of manifolds and densities by simple injective flows," *arXiv preprint arXiv:2110.04227*, 2021. **4**
- [57] K. Kothari, M. de Hoop, and I. Dokmanić, "Learning the geometry of wave-based imaging," *Advances in Neural Information Processing Systems*, vol. 33, pp. 8318–8329, 2020. **5**
- [58] D. P. Kingma and J. Ba, "Adam: A method for stochastic optimization," *arXiv preprint arXiv:1412.6980*, 2014. **5**
- [59] M. Abadi, P. Barham, J. Chen, Z. Chen, A. Davis, J. Dean, M. Devin, S. Ghemawat, G. Irving, M. Isard *et al.*, "Tensorflow: A system for large-scale machine learning," in *12th {USENIX} symposium on operating systems design and implementation ({OSDI} 16)*, 2016, pp. 265–283. **5**
- [60] P. M. van den Berg, A. Van Broekhoven, and A. Abubakar, "Extended contrast source inversion," *Inverse problems*, vol. 15, no. 5, p. 1325, 1999. **6**
- [61] Y. LeCun, L. Bottou, Y. Bengio, and P. Haffner, "Gradient-based learning applied to document recognition," *Proceedings of the IEEE*, vol. 86, no. 11, pp. 2278–2324, 1998. **6**